THE ROLE OF FOLDING IN THE DEGRADATION OF BALLISTIC FIBERS

Walter G. McDonough, Gale Holmes, Jae-Hyun Kim, Derek Ho
National Institute of Standards and Technology
Polymers Division,
Gaithersburg, MD 20899-8541

ABSTRACT

Research has indicated that the folding of ballistic fibers comprising soft body armor may be a factor in the performance deterioration that has been observed. To quantify the impact of this failure mechanism on body armor performance, an apparatus was designed and built to simulate the folding that may occur in the ballistic fibers while the vest is in use. This device systematically folds woven fabric and yarns of ballistic fibers to enable an assessment of the impact of folding on ballistic fiber properties. After cycling a piece of woven poly(benzoxazole) (PBO) fabric for 80,000 cycles, a 41 % reduction in the ultimate tensile strength and strain to failure of the PBO fibers was observed. These results were also reflected in data obtained from small angle x-ray scattering (SAXS) where the long range order of the fiber structure is changed by the folding process. Preliminary failure analysis using scanning electron microscopy (SEM) on tested fibers also revealed changes in failure morphology.

KEY WORDS: Materials – Fabrics/Knitted/Stitched, Mechanical/Physical Properties, Testing/Evaluation

1. INTRODUCTION

Soft body armor has been credited with saving over 3,000 lives. One factor in the performance deterioration observed in worn soft body armor may be the folding of the ballistic fibers. In an attempt to quantify the impact of this mechanism, an apparatus was designed and built to simulate this folding. A long-term goal of the folding research on ballistic fibers is the development of a controlled procedure for simulating the folding that occurs in an actual vest during various stages of its proposed lifespan. This type of procedure would then allow ballistic fiber tests to be performed on body armor whose wear and deformation history are known. Such tests on controlled materials should help to establish the link between use and life expectancy of the body armor.

The apparatus described in this report was designed to fold individual yarns and single and multiple layers of woven fabrics of ballistic fibers by using servo-hydraulic testing equipment that is often available in laboratories that perform fatigue testing of materials. Since the concept is new, a major goal was to incorporate sufficient flexibility into the design to allow most of the deformation parameter space that occurs during actual use to be systematically probed, with the end result being an optimized and relevant deformation protocol. Furthermore, the use of commercial off-the-shelf testing equipment, such as the servo-hydraulic testing equipment, should facilitate peer review and use by others.

2. MOTIVATION: THE SINGLE FOLD TEST

The research of Cunniff and Auerbach (1) has shown that, within the elastic limit, a correlation exists between the ballistic fiber properties and ballistic performance if the fiber properties are decoupled from the vest construction parameter of areal density. That is, the material properties of the fiber are separated from the vest construction parameters known to depend on a manufacturer's vest design. From their research, the correlation between ballistic performance and the mechanical properties of the active fiber is quantified by $(U^*)^{1/3}$ of equation 1. Therefore, $(U^*)^{1/3}$ is a theoretical parameter that estimates the maximum velocity of a bullet that the fibers of a vest can stop and is independent of vest construction. This equation has also been derived theoretically by Phoenix and Porwal (2,3).

$$\left[U^*\right]^{1/3} = \left[\frac{\sigma_f^u \varepsilon_f^u}{2\rho}\sqrt{\frac{E_{1f}}{\rho}}\right]^{1/3} \tag{1}$$

where

σ_f^u is the fiber ultimate axial tensile strength (UTS),

ε_f^u is the fiber ultimate tensile strain,

ρ is the fiber density, and

E_{1f} is the longitudinal linear elastic fiber modulus.

In a previous publication, it was shown that a *modified* single fiber test (*m*-SFT) (4), based on ASTM C1557-03 (5), could be used to obtain the fiber properties for the above equation. In addition it was shown that this test could detect changes in mechanical properties, presumably arising from ultraviolet (UV) exposure and hydrolytic action that indicate, according to equation 1, a reduction in ballistic performance. Since it is probable that mechanically induced degradation will induce subtle changes in ballistic fiber properties, a preliminary study was conducted where 50 fibers were extracted from a single yarn of virgin poly(benzoxazole) (PBO) fibers and subjected to a single fold. In this work the visible damage induced by the single fold was accompanied by changes in the fiber properties as measured by the m-SFT (6). The 10 % reduction in strain-to-failure and tensile yield strength observed in the single fold test were significant enough to warrant further study, with the ultimate goal being to link observable reductions in ballistic performance to measurable molecular or microstructural changes in the ballistic fibers (see Table 1).

3. EXPERIMENTAL

3.1 Folding Apparatus Design and Operation The design was motivated by the desire to use the controlled fatigue testing features inherent in most servo-hydraulic test machines. To minimize damage to the servo-hydraulic machine by the apparatus, the device was designed to fit on a 250 kN (55 kip) Model 810.25 MTS machine equipped with a 158.5 mm (6.25 in) diameter piston rod. To convert the linear motion of the servo-hydraulic machine to rotational motion, a bracket was fitted to the piston rod that contained a spur gear and rack.

To effect the folding of the ballistic fiber material, a two-piece clamshell design is employed (see Figure 1). To minimize mass, most of the apparatus is constructed using aluminum, except where otherwise specified. The lower plate is connected to a platform that attached to the servo-hydraulic machine through the column mounting brackets. An interchangeable folding rod with diameter of 6.35 mm was constructed out of stainless steel and attached to this plate. The upper plate is attached to a stainless steel rod that is turned at each end to conform to the required bore size of the spur gear. The top plate is attached to the platform using two base-mount ball bearings that accommodate a shaft. Each plate is equipped with Teflon sheets to minimize friction between the ballistic material and the plate surface. To hold the fabric or yarn in place each plate is equipped with a sliding bracket. Each sliding bracket is held in place by two stainless steel rods that attach to constant force springs.

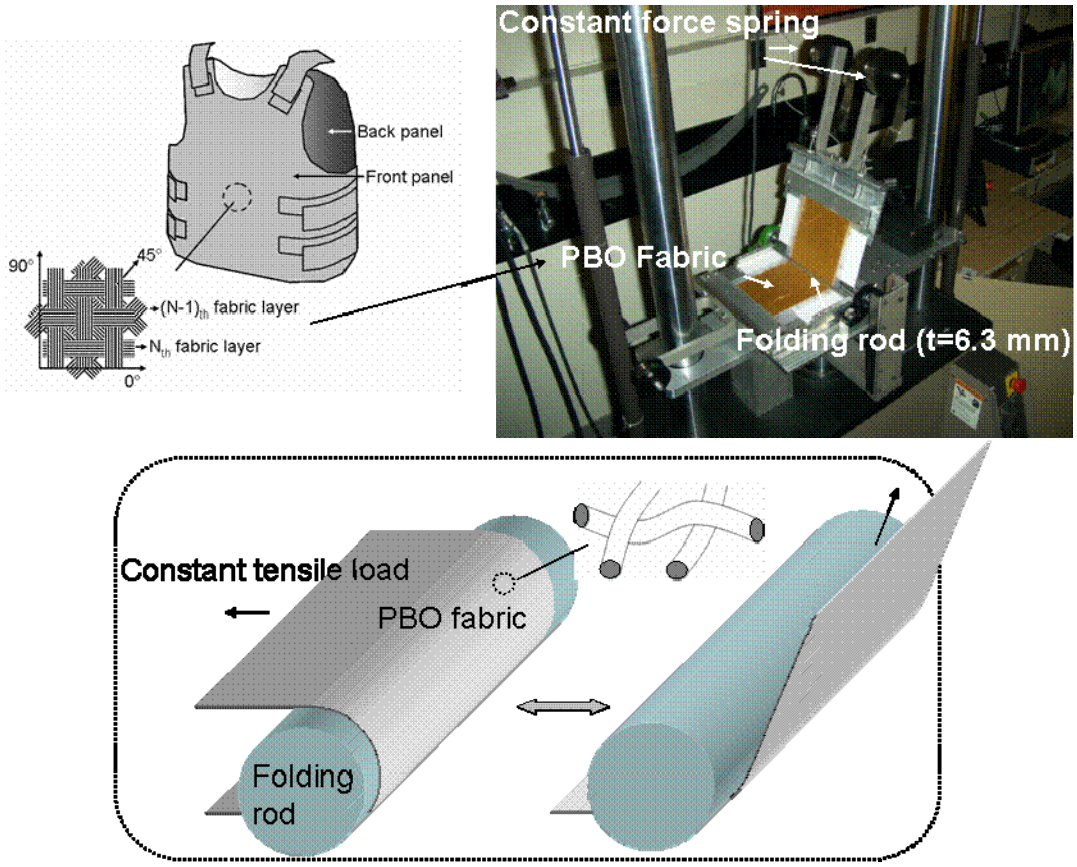

Figure 1. Schematic of the continuous folding apparatus and folded region of the PBO fabric.

3.2 Modified Single Fiber Fragmentation Test (m-SFT) This test procedure was described in detail in a previous publication (4). The maximum standard uncertainty in the strain measurements for a 6 cm gauge length specimens was determined to be 0.0001. The standard uncertainty in the load cell at 100 g was 0.001 g.

3.3 Small Angle X-ray Scattering (SAXS) Small-angle x-ray scattering is a well-known technique to characterize the structure of materials over length scales of sub-nanometers (nm) to 100 nm, depending on the instrumentation. In this work, the SAXS configuration with copper radiation (SAXS-Cu) is in a conventional pinhole (PH) collimation geometry with three pinholes, PH1 = the source pinhole, PH2 = the beam defining pinhole, and PH3 = the sample pinhole, as shown in Figure 2. The source-to-sample distance (SSD) is fixed at 122.5 cm, whereas the sample-to-detector distance (SDD) varies from 26 cm to 406 cm, yielding an overall wave vector Q (where $Q = (4\pi/\lambda)\sin\theta$, λ is the x-ray wavelength, and 2θ is the scattering angle) range of 0.05 nm^{-1} to 14.90 nm^{-1}, probing a length scale range of ca. 0.42 nm to 126 nm (7). $D = 2\pi/Q$ is the corresponding length scale in the real space (8-9). The $K\alpha_1$ wavelength of Cu is 0.15406 nm at 8.04 keV. A two-dimensional (2-D) 30 cm × 30 cm image plate is used for the data acquisition (10). The beam from the source is parallel through Osmic multilayer confocal optics.

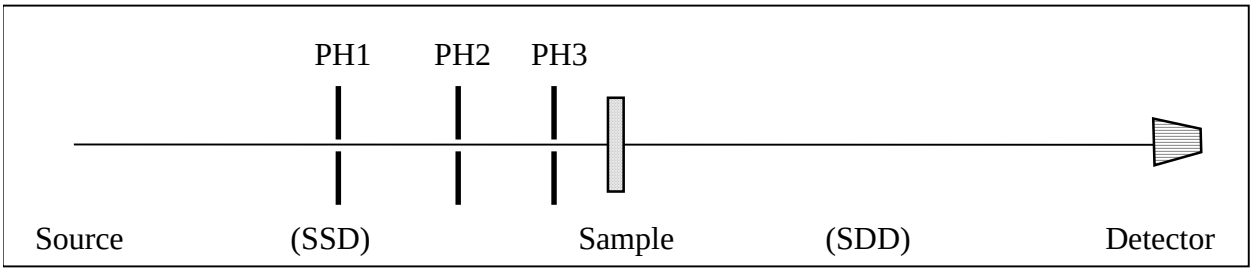

Figure 2. Schematic shows the pinhole geometry for SAXS-Cu.

In this study, a SAXS-Cu setup with SDD = 406.0 cm for the low-Q scans and 26 cm for the high-Q measurements, the detector pixel size = 200 μm × 200 μm as well as PH1 = 400 μm, PH2 = 200 μm and PH3 = 700 μm in diameter, yielding an x-ray beam size of ca. 300 μm on the sample, was used for the measurements. The fibers were in a bundle mounted vertically on a sample holder and probed in the transmission mode at room temperature under vacuum.

3.4 Scanning electron microscopy (SEM) A scanning electron microscope was used in order to investigate changes in surface morphology after cyclic folding and also to characterize the tensile fracture surface of PBO fibers. For investigating the effect of the folding on the PBO fibers, PBO strands were carefully collected from unfolded and folded fabrics respectively, and these strands were placed on a carbon conductive tape. The fracture mechanisms of PBO fibers after folding, and tensile fracture using the m-SFT test were also characterized by placing these specimens on carbon tape. These SEM samples on the carbon tapes were then coated by gold to achieve high resolution images.

4. RESULTS AND DISCUSSIONS

The results from the m-SFT (4) are shown in Table 1. From the results, one can see the reduction in the theoretical ballistic performance parameter as the number of folds increases. A 14 % reduction in fiber properties was observed after 5,500 (5.5 K) cycles, while a more rigorous 80,000 (80 K) cycle folding caused a 40 % reduction.

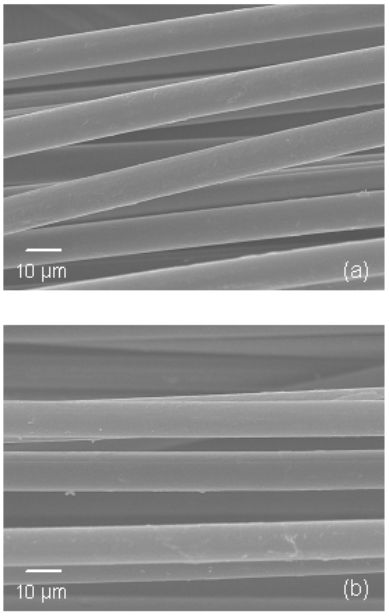

Figure 3. SEM image of the 5,500 (a) and 80,000 (b) cycle fold PBO fibers.

Figure 3 shows an SEM image of PBO fibers after 5,500 and 80,000 cyclic folding. No damage exists on the surface of the fibers. This suggests that the folding device used in this study generates internal damage and avoids the effect of friction with the folding rod. Figure 4 shows tensile stress-strain behavior of the PBO fibers with similar fiber diameters before and after cyclic folding. Regardless of the cyclic folding, all tested fibers showed non linear stress-strain behavior until fracture. This unique behavior is a well known property for as-spun PBO fibers. It is known that the degree of the crystallite orientation between core and skin region in the as-spun PBO fiber is significantly different, so the core region with poor chain orientation improves more than that of the skin region under tension. As a consequence, the different stress response of these two regions causes the non linear tensile behavior at the higher strain (11-12). Compared to the similarity of the global tensile behavior among the samples, the tensile behavior of the 5.5K folded fibers are more scattered than the other two fibers (i.e., controlled and 80K folded) at the higher strain region. This difference of the 5.5K folded fibers implies that the defect size distribution in the fiber is more significant than the other two fibers. Therefore, the 5.5K folded fibers are considered to contain various sizes of defects (i.e., defect size distribution) in each single fiber by folding, while the controlled and 80K folded fibers are considered to have no significant size distribution of the flaws in the single fiber. Typically, PBO fibers contain needle like internal voids having approximately 2.4 nm diameter which are connected each other

through cracks or openings between micro fibrils (13). During the folding process, two stress components at the folded region, tensile and compressive, can be simultaneously applied to the

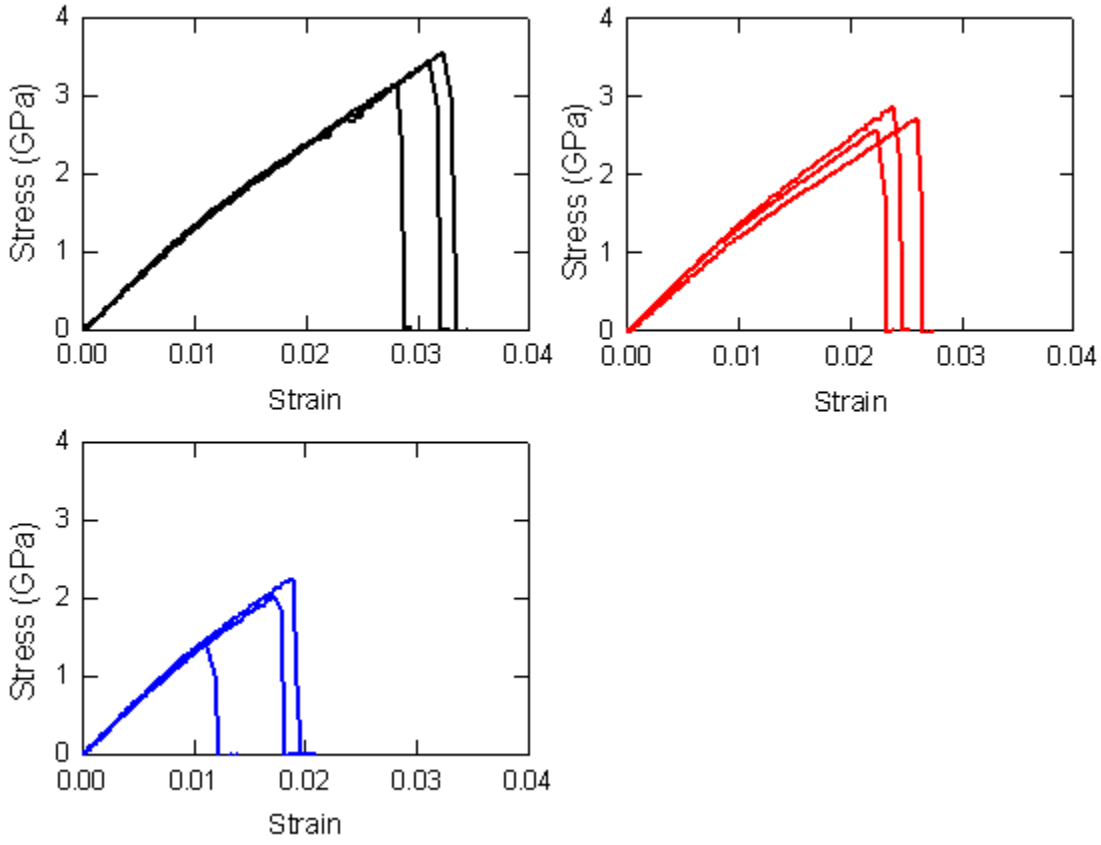

Figure 4. Tensile stress-strain behavior of the unfolded (—), 5,500 (—) and 80,000 (—) PBO fibers.

intrinsic transverse cracks among the micro-voids. Tensile stresses that move from the neutral plane to the outer plane at the folded region can develop crack growth in the transverse direction of the fiber, and eventually reach a critical size by linking the intrinsic micro-voids to the transverse direction of the fiber. Therefore, the failure behaviors of fibers change from fibrillar to brittle at the folded region.

In Figure 5, fracture surfaces of the fibers also show a transition from longitudinal fiber crack propagation (fibrillation) to transverse crack propagation. The energy needed to form a crack increases with crack growth and then decreases after the crack size exceeds a critical size. The crack exceeding the critical size causes rapid crack propagation. So we speculate that the cracks of the 80K fibers, which were initiated at the edge of the internal voids, are sufficiently grown by folding. These flaws can quickly reach the critical size, so that transverse crack growth is dominant. Therefore, defects introduced by the cyclic folding appear to be the key parameter that

decreases the tensile strength of the fibers. It is known from fundamental studies associated with the yarn test that cracks perpendicular to the fiber axis can be formed by twisting the yarn specimens (14).

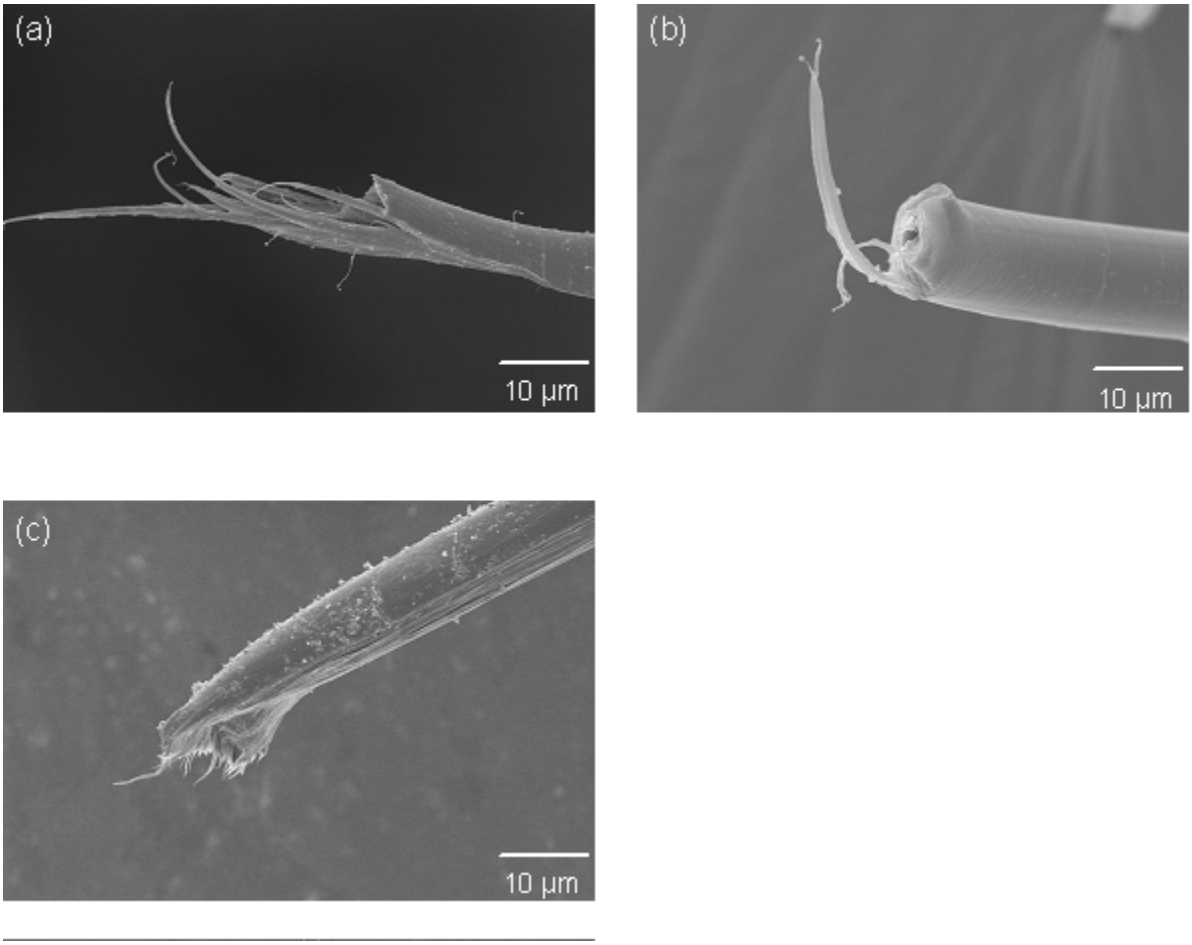

Figure 5. Fracture surface of the (a) unfolded, (b) 5,500, and (c) 80,000 PBO fibers.

In addition to the techniques introduced and discussed above, the PBO fibers studied were also probed by SAXS-Cu to examine the folding treatment effects on the fiber structures down to the sub-nanometer level. Figure 6 demonstrates the 2-dimensional (2-D) raw SAXS-Cu data from one of the fiber samples at both low and high Q. As mentioned earlier in this paper, the bundle of fibers were mounted and probed vertically in the x-ray beam, resulting in an anisotropic 2-D scattering pattern on the detector along the horizontal axis from the individual crystals aligned within the fibers vertically. The 2-D raw data were then averaged both horizontally (H) and vertically (V) within a rectangle of 550 pixels long and 26 pixels wide centered at the beam center and normalized by the corresponding transmission to yield the I(Q) versus Q profile for both low and high Q. I(Q) is the scattered intensity at that specific Q.

SAXS-Cu profiles from the 5.5K and 80K folded/unfolded fiber samples reduced horizontally and vertically are presented in Figure 7, with an experimental uncertainty less than 1 %. Overall, the SAXS-Cu data attest that the folding process has no effects on both the 5.5 K and 80 K fibers along the vertical fiber orientation/alignment, reflected by the horizontally reduced SAXS profiles, over the Q (length scale) range probed, whereas it slightly affects/changes the structure in the direction perpendicular to the vertical fiber orientation/alignment on a large length scale

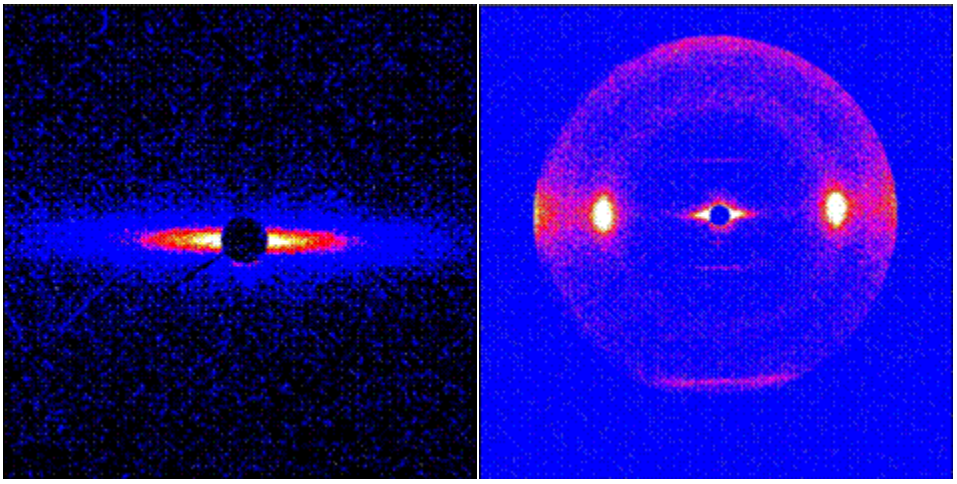

Low Q **High Q**

Figure 6. 2-D SAXS-Cu images from the unfolded PBO fibers.

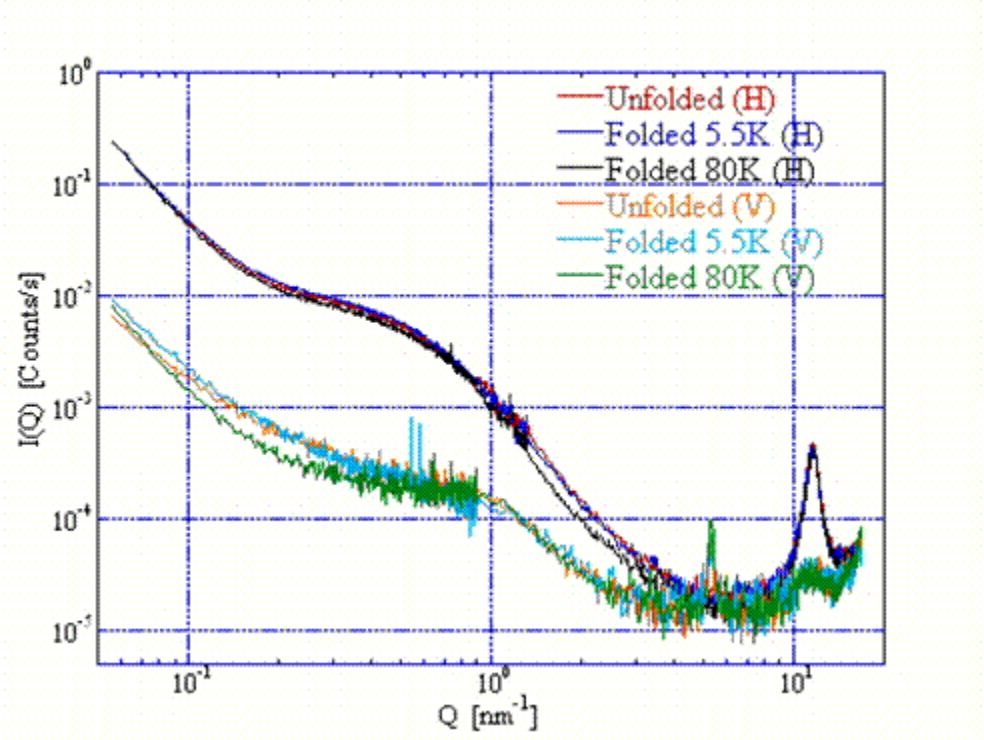

Figure 7. SAXS-Cu profiles from the PBO fibers.

(sub-micrometer and/or micrometer orders), corresponding to the low-Q regime in Figure 7, in the vertically reduced SAXS profile from the 80K fibers. Since the stress generated from the constant force spring to the fabric is sufficiently low to avoid the premature tensile fracture of the fibers, these results showing no damage of the PBO crystal unit along the fiber alignment are not surprising.

5. CONCLUSIONS

The folding apparatus as designed can consistently fold woven fabrics and yarns, and successfully create internal damage of the PBO fibers. Tensile strengths of the folded fibers were decreased with the number of folds. The 5,500 cycle folding showed a 14 % reduction and more rigorous 80,000 cycle folding caused a 41 % reduction relative to the properties of the woven fabric. SAXS analysis, which shows no PBO crystalline damage, suggests the internal flaw growth occurs through the intrinsic micro-voids. More testing is planned to determine the optimum and relevant testing conditions required to simulate the impact of folding over a period of (5 to 10) years of use. Further tests are underway to quantify the direct mechanism of mechanical degradation.

5. ACKNOWLEDGEMENT

The authors wish to thank the National Institute of Standards and Technology Office of Law Enforcement and Standards (NIST-OLES) under the auspices of the National Institute of Justice (NIJ) for funding this work. Certain commercial materials and equipment are identified in this paper in order to specify adequately the experiment procedure. In no case does such identification imply recommendation by the National Institute of Standards and Technology nor does it imply that the material or equipment identified is necessarily the best available for this purpose.

6. REFERENCES

1. P.M. Cunniff and M.A. Auerbach, 23rd. Army Science Conference, AO-04, Orlando, Florida, (2002).
2. S.L. Phoenix and P.K. Porwal, International Journal of Solids and Structures, 40**,** 6723 (2003).
3. S.L. Phoenix and P.K. Porwal, International Journal of Fracture, 135, 217 (2005).
4. J.H. Kim, W.G. McDonough, W. Blair and G.A. Holmes, Journal of Applied Polymer Science, Submitted (2006).
5. ASTM C 1557-03. Philadelphia, PA: ASTM (2003).
6. W.G. McDonough, J.H. Kim, N.Y. Brandenburg, W. Blair and G.A. Holmes, SAMPE 2007 Technical Symposium, CD-ROM 6 (2007).
7. D.L. Ho, E.K. Lin, C.Q. Wang, R.L. Jones, W.-L. Wu and S.W. Barton, (2007).
8. J.S. Higgins and H.C. Benoît, Polymers and Neutron Scattering, Oxford, New York, (1994).

9. R.-J. Roe, Methods of X-Ray and Neutron Scattering in Polymer Science, Oxford, (2000).
10. Rigaku R-Axis IV^{++} CE Marking System (2-D Image Plate) Instruction Manual (Manual Number ME11526A05).
11. R.J. Davies, M.A.Montes-Moran, C. Riekel, and R.J. Young, Journal of Materials Science, 36, 3079, (2001).
12. R.J. Davies, M.A.Montes-Moran, C. Riekel, and R.J. Young, Journal of Materials Science, 38, 2105, (2003).
13. T. Kitagawa, H. Murase, and K. Yabuki. Journal of Polymer Science: Part B, 36, 39, (1998).
14. T. Kitagawa, K. Yabuki, and R.J.Young, Polymer, 42, 2101, (2001).

Table 1 Results from the m-SFT tests

Sample	Diameter, μm	Modulus, GPa	Failure Strain, %	Tensile Strength, GPa	Theoretical Ballistic Performance m/s
Virgin Fiber (VF)	12.5 ± 0.2	163 ± 10	3.53 ± 0.45	4.46 ± 0.50	**802**
Single Fold VF	12.6 ± 0.3	156 ± 12	3.18 ± 0.50	3.98 ± 0.53	**740**
Woven Fabric (WF)	13.1 ± 0.3	143 ± 10	2.97 ± 0.39	3.36 ± 0.57	**674**
Folded WF (5.5K Cycles)	13.0 ± 0.3	146 ± 9	2.50 ± 0.45	2.89 ± 0.42	**607**
Folded WF (80K Cycles)	13.3±0.4	135±8	1.74±0.32	1.99±0.30	**472**